

Magnetic properties of endohedral fullerenes: applications and perspectives

Panagiotis Dallas ^{1*}, Reuben Harding ¹, Stuart Cornes ¹, Sapna Sinha ¹, Shen Zhou ¹, Ilija Rašović ¹, Edward Laird ^{1,2} and Kyriakos Porfyrakis ^{1*}

¹Department of Materials, University of Oxford, OX1 3PH

²Department of Physics, Lancaster University, Lancaster, LA1 4YB, United Kingdom

- panagiotis.dallas@materials.ox.ac.uk; kyriakos.porfyrakis@materials.ox.ac.uk

Keywords: atomic clocks, frequency standards, contrast agents, quantum devices, peapods.

Abstract

In this chapter we discuss the magnetic properties of endohedral fullerenes, both those with an atomic nitrogen and those with a metal or metal cluster (endohedral metallofullerenes (EMFs) incarcerated inside the cage. We highlight newly developed applications, such as their use as frequency standards for atomic clocks, alongside the previously explored and studied fields of quantum information processing, molecular magnets, photoswitchable rotors, ferromagnetic ordering on substrates, spin probes, magnetic resonance imaging and spintronics. In the chapter we also provide insights on the fundamental principles behind the magnetic properties of endohedral fullerenes and we discuss new prospects for their synthesis and applications.

Introduction.

Small children, when presented with hollow toys, will instinctively try to place different kinds of object inside them. Chemists behave in much the same way. Soon after fullerene molecules were discovered (Kroto1985) it was natural to ask whether the empty space inside them could host other atoms or molecules. Within a decade the answer was known to be “yes”. This class of molecules are the endohedral fullerenes.

Although fullerene molecules are not magnetic, the incarcerated species may be. Endohedral fullerenes thus combine magnetic properties from the incarcerated species with chemistry that is often similar to that of empty fullerene molecules. This allows unique functionality that cannot be attained in any other material. The magnetic properties of endohedral fullerenes offer advantages in two ways. Firstly, the fullerene protects the incarcerated species from its environment. This is beneficial when long spin lifetimes are desired, and possible applications are for quantum information and for atomic clocks. Secondly, the fullerene protects the environment from the incarcerated species. This allows otherwise toxic spin markers to be used inside the human body.

This critical review introduces the magnetic behaviour of this class of materials with a view to possible applications. The remainder of this introduction summarizes the structure and synthesis of endohedral fullerenes. Section 1 describes basic magnetic behaviour in nanomaterials and on substrates. Section 2 introduces peapods: chemically assembled spin arrays. Section 3 focuses on biomedical applications of endohedral fullerenes. Section 4 explains the uses of endohedral fullerenes as spin qubits. Section 5 introduces a new research topic, endohedral fullerenes for atomic clocks. We conclude by discussing challenges and future directions for the field.

Spin-bearing endohedral fullerenes come in two classes. The incarcerated species can be a metal atom or a metallic cluster (usually a transition metal or a rare earth), in which case the molecule is known as an endohedral metallofullerene (EMF). Alternatively, the incarcerated species can be a single atom from Group V (either N or P). The chemical formula is denoted $X@C_n$, where X is the incarcerated species and n is the number of atoms in the cage. Some of the most important endohedral fullerenes are listed in Table 1. These two classes behave in quite different ways. In the metallofullerenes, the incarcerated species generally interacts strongly with the cage, forming a charge transfer complex. The incarcerated species usually

sits off-centre in the cage, and may have more than one stable position, leading to multiple isomers. By contrast, Group V endohedral fullerenes have almost no charge transfer, and the incarcerated atom sits in the centre (Plakhutin, B.N. 2005, Lu, X. 2005).

Different incarcerated species are compatible with different encapsulation structures. Both N and P are small enough to fit inside a C_{60} cage. This cage is nearly spherically symmetric (to be precise, it is icosahedral), and the spin therefore experiences a nearly isotropic environment. This symmetry contributes to the excellent spin coherence in these materials. While metals may be encapsulated in smaller cages, such as C_{60} , C_{70} or C_{76} the solubility of these elusive fullerenes is very low and it is impossible to isolate them in respectable quantities. In contrast, EMFs with larger cages, for example C_{80} , C_{82} or C_{84} have been isolated and thoroughly studied. Some of these larger fullerenes, for example C_{82} , deviate substantially from spherical shape. The combination of charge transfer to the cage (allowing the electron spins to interact with the environment) and lower symmetry (meaning that the spins are perturbed by tumbling motion of the cage) make the spin lifetimes of metallofullerenes lower than the group V endohedral fullerenes. Figure 1 shows the structure and spin resonance spectrum of selected molecules.

Several ways to synthesize endohedral fullerenes are known, and three techniques have been particularly well developed. Metallofullerenes can be made by ablating graphite that has been doped with the desired species. This ablation is achieved either using powerful lasers, or by arc discharge. This technique does not so far work for Group V endohedral fullerenes; instead, the molecules are synthesized using ion implantation to inject the N or P atom into an effusing beam of C_{60} molecules (Murphy, T. 1996). In all these techniques, the ratio of endohedral fullerene to fullerene in the product is low (typically less than 1%).

$^{14}\text{N}@C_{60}$	3/2	2.0021	1	{5.70 G}(Pietzak 1998)
$^{15}\text{N}@C_{60}$	3/2	2.0020	1/2	{7.98 G}(Pietzak 1998)
$^{31}\text{P}@C_{60}$	3/2	-	1/2	49.2 G (Knapp 1998)

$^{45}\text{Sc}@C_{82}$ (I)	1/2	1.9999	7/2	3.82 G (Inakuma 2000)
$^{45}\text{Sc}@C_{82}$ (II)	1/2	2.0002	7/2	1.16 G (Inakuma 2000)
$^{45}\text{Sc}@C_{84}$	1/2	1.9993	7/2	3.78 G (Inakuma 2000)
$^{89}\text{Y}@C_{82}$ (I)	1/2	2.0006	1/2	0.49 G (Kikuchi 1994)
$^{89}\text{Y}@C_{82}$ (II)	1/2	2.0001	1/2	0.32 G (Kikuchi 1994)
$^{139}\text{La}@C_{82}$ (I)	1/2	-	7/2	1.15 G (Yamamoto 1994)
$^{139}\text{La}@C_{82}$ (II)	1/2	-	7/2	0.83 G (Yamamoto 1994)
$^{45}\text{Sc}_3\text{C}_2@C_{80}$	1/2	1.9985	[21/2]	6.51 G (Shinohara 1994)

Table 1. Selected endohedral fullerenes, listing electron and nuclear spin quantum numbers, electronic g factor and hyperfine coupling. The nuclear spin value given for $^{45}\text{Sc}_3\text{C}_2@C_{80}$ is an effective value due to coupling between the identical Sc atoms, each with nuclear spin $I=7/2$. Molecular isomers are labelled by roman numerals, starting with the major isomer labelled (I).

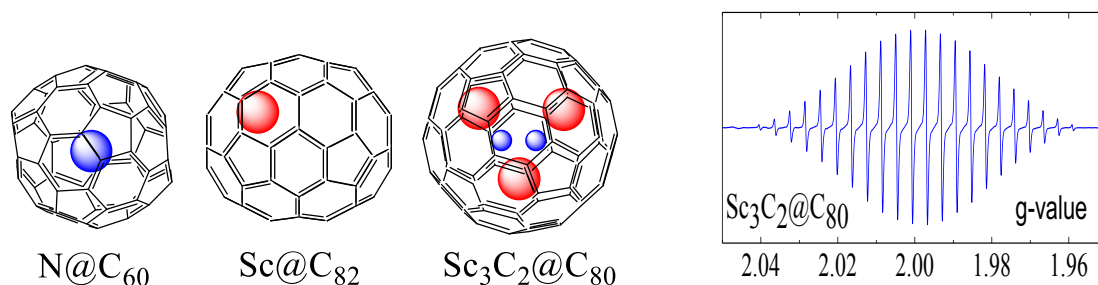


Figure 1. Structures of $\text{N}@C_{60}$, $\text{Sc}@C_{82}$ and $\text{Sc}_3\text{C}_2@C_{80}$. The EPR spectrum of $\text{Sc}_3\text{C}_2@C_{80}$. The number of resonances for each molecule is $N = 2I_{\Sigma} + 1$, where I_{Σ} is the sum of the nuclear spins. For example in $\text{Sc}_3\text{C}_2@C_{80}$, three $I = 7/2$ atoms combine to give $I_{\Sigma} = 21/2$.

1. Magnetic properties of EMFs.

1.1. Nanomagnetic materials.

The paramagnetic properties of EMFs have attracted attention due to the presence of spin active transition metals and rare earth metals exhibiting different hyperfine couplings (HFC) and the observation of ferromagnetic coupling with various functional molecules and substrates. Since the metal cation or the metal cluster can occupy different positions inside the

cage, different g values and HFCs should be anticipated. Examples of transition metals with sharp electron paramagnetic resonance (EPR) signals and long spin lifetimes are scandium, yttrium and lanthanum. Rare earth elements such as gadolinium and erbium have applications in biomedicine as contrast agents and in telecommunications, respectively. While erbium EMFs are appealing for optical communications because characteristic 1520 nm emission from the erbium ion falls within the telecommunications window, their EPR spectra are broad due to the location of the f-orbital electrons (Bondino 2006). Previous works debate the location of the spin and the effect of the rotation of the metal cluster inside the cage, with both having a significant influence on the resulting EPR spectrum at lower temperatures. For example, the two isomers of $\text{Sc}@C_{82}$ and of $\text{Y}@C_{82}$ exhibit different hyperfine couplings and g values despite the fact that the cluster is inside the same, C_{82} , cage [Inakuma 2000]. For a comprehensive analysis of the magnetic properties of endohedral metallofullerenes, see the review by Zhao 2015. More complicated EPR spectra can be observed in scandium carbide $\text{Sc}_3\text{C}_2@C_{80}$, which exhibits a unique diamond shaped EPR signal consisting of 22 lines (Roukala 2017). This EMF has been used for the synthesis of molecular magnetic switchable dyads when connected with an organic molecule bearing a nitroxide radical. [Figure 2, Wu 2015] A similar EMF-nitroxide radical system based on a dysprosium EMF was used as a molecular compass with position sensitive magnetoreception ability. EPR measurements show that the dipole–dipole interactions depend on the orientation of the Dy_3N cluster inside the cage. [Li 2017]

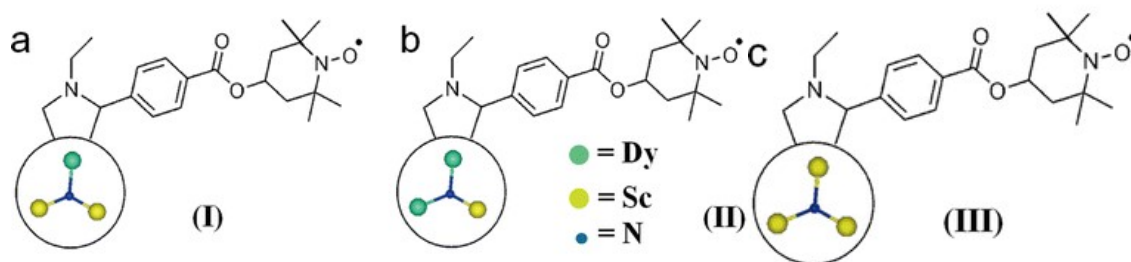


Figure 2. A dyad consisting of $\text{DySc}_2\text{N}@C_{80}$ and $\text{Dy}_2\text{ScN}@C_{80}$ and a nitroxide radical. Reproduced with permission from Wu 2016.

The rotation of ^{45}Sc inside the C_{80} cage and the dynamics of the fullerene and the endohedral cluster dictate the temperature dependence of the EPR spectrum. This rotation is found to be hindered by functionalization of the external surface. The observed temperature dependence is well explained by density functional theory (DFT), which predicts three-axis rotation of the carbide at high temperatures but only two-axis rotation at low temperatures. Detailed analysis of the EPR signals of scandium endohedral metallofullerenes was performed and presented by the Shinohara group. [Inakuma 2000] Three monometallic scandium incarcerating fullerenes, namely the two isomers of $\text{Sc}@C_{82}$ and $\text{Sc}@C_{84}$ were studied in a temperature range of 150 K to 270 K. Unique spin dynamics are observed in EMF clusters. Furthermore, the creation of a radical on the surface of EPR silent EMFs can also give rise to an EPR spectrum with hyperfine features. [Elliott 2013]

Ferromagnetic interactions of endohedral fullerenes with organic molecules, such as copper porphyrin [Hajjaj 2011], or a metallic substrate have been investigated—Svitova *et al.* (Svitova 2014) reported the formation of an inclusion complex, where $\text{La}@C_{82}$ is incorporated between two Cu(II) porphyrin units. These studies demonstrated two different types of interactions: from a ferromagnetic coupling in the case of *cyclo*- $[\text{P}_{\text{Cu}}]_2$ acting as the inclusion host, to a ferromagnetic coupling for a *cage*- $[\text{P}_{\text{Cu}}]_2$ cage host. Due to the long magnetic relaxation times, similar to those of single-molecule magnets, some dimetallic EMFs have been considered for spintronics applications.

1.2. Magnetic fullerenes on substrates.

With respect to their magnetic properties when EMFs form a layer on metallic substrate, interactions between the two components might take place. As an example, Hermanns 2013 demonstrated the coupling of a $\text{Gd}_3\text{N}@C_{80}$ EMF to a nickel substrate. The Gd magnetization is antiparallel to the Ni at low temperatures and parallel at high temperatures—the Gd atoms of the fullerenes coupled with a ferromagnetic alignment to each other. By X-ray magnetic circular dichroism (XMCD) measurements they revealed the magnetic coupling while the close self-assembly of the fullerenes was proven through STM images on a $\text{Cu}(001)$ substrate. Dy_2S is a class of endohedral metallofullerenes, synthesized using Dy_2S_3 as the inorganic metal component added in the graphite rods (Chen 2017), These EMFs exhibit permanent magnetization as proven by hysteresis loops while DC and AC susceptibility measurements were employed for determining the magnetization relaxation times. In Figure 3 we present the magnetization curves of the following endohedral metallofullerenes, $\text{Dy}_2\text{S}@C_{82}-C_{3v}(8)$, (c) $\text{Dy}_2\text{C}_2@C_{82}-C_s(6)$, and (d) $\text{Dy}_2\text{S}@C_{72}-C_s(10528)$. In very low temperatures a clear hysteresis is observed in the curves of $\text{Dy}_2\text{S}@C_{82}-C_s(6)$, (b) $\text{Dy}_2\text{S}@C_{82}-C_{3v}(8)$.

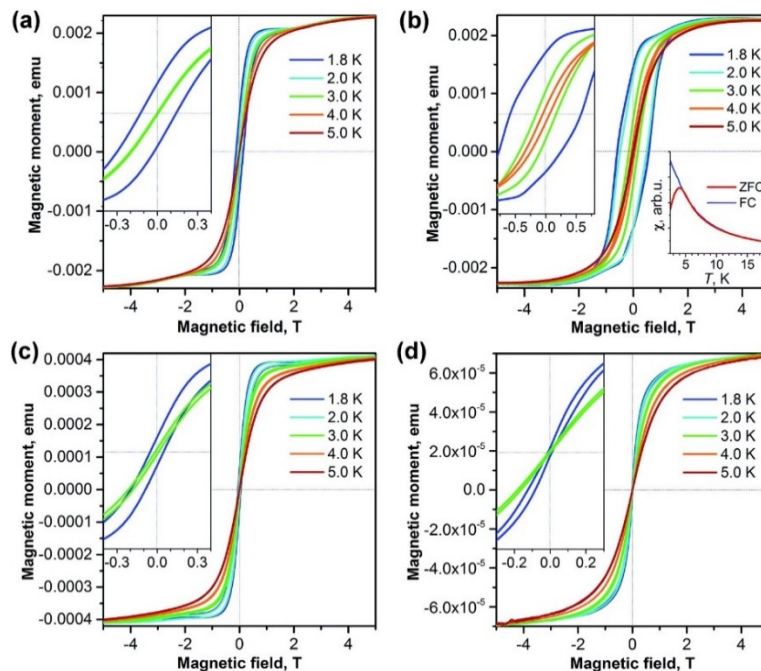


Figure 3. Magnetization curves for (a) Dy₂S@C₈₂-C_s(6), (b) Dy₂S@C₈₂-C_{3v}(8), (c) Dy₂C₂@C₈₂-C_s(6), and (d) Dy₂S@C₇₂-C_s(10528). The loops were recorded at $T = 1.8\text{--}5$ K. Reproduced with permission from (Chen 2017).

2. Peapods: Spin-active EMFs inside Carbon Nanotubes

Electron paramagnetic resonance (EPR) is a powerful tool for studying and understanding the properties and behaviour of electron spins. Through detailed EPR analysis we can probe the structure, paramagnetic states and highest occupied molecular orbital (HOMO) and lowest unoccupied molecular orbital (LUMO) density distributions. Endohedral fullerenes give rise to some of the narrowest EPR lines to be detected under normal atmospheric conditions. For that reason, endohedral metallofullerenes may be potential candidates for quantum information processing devices, with EPR as a tool for controlling qubits. The incarcerated electron spins offer both long coherence times and the potential for controlled spin-spin interactions.

In a carbon nanotube (CNT) peapod, fullerenes are arranged in a chain inside a nanotube. This offers a way to make a spin register – an array of metallofullerene spins with controlled interactions. Electrons delocalised on the carbon nanotube can themselves encode quantum bits (qubits) (Laird 2013), and could ultimately act as both a spin bus and a readout line (Benjamin 2006). The magnetic properties depend not only on the EMF species, (Kitaura, R.2007), but also on their concentration inside the peapods (Figure 4, Cirić, L. 2008). The EPR lines were deconvoluted in two components, a narrow and a broad component. In order to control the distance between the spin active components, C₆₀ have been used as a spacer between La@C₈₂ molecules inside a single-walled CNT. Below 70 K, the g_B -factor of the broad EPR component rapidly decreases as the relative content of the EMFs increases and *vice versa* for measurements carried out at temperatures above 70 K. Spin loss can pose drawbacks while fabricating nano-peapods, and this should be taken into account when considering these hybrid materials as

potential candidates for spintronics and quantum devices. An important point to note when considering electron spins of EMFs for quantum applications is that all the EPR measurements carried out so far on fullerene spins have been performed on ensembles of molecules.

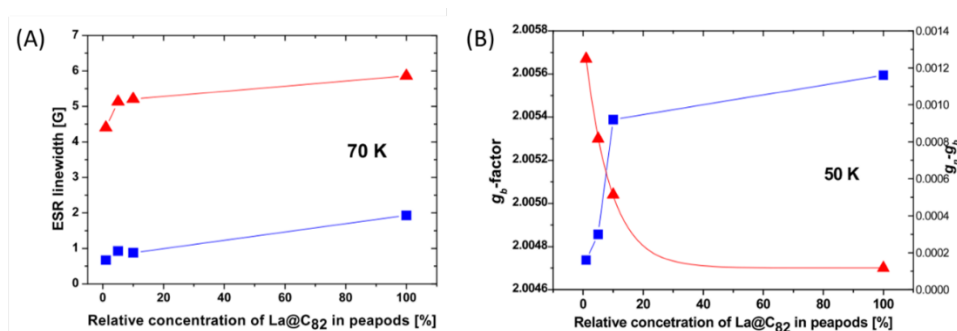


Figure 4. (A) Shows the line width of the narrow (blue) and the broad (red) components of the EPR spectrum at different La@C₈₂ concentrations. (B) Relative content of the EMF in peapods, along with the evolution of the g_b factor of the broad ESR spectrum. Reproduced with permission from (Ćirić, L. 2008).

3. Biomedical applications.

Derivatives of the gadolinium-containing endohedral metallofullerenes (Gd-EMFs) have been proposed as the next generation of T_1 contrast agents for ¹H magnetic resonance imaging (Ghiassi *et al.*, 2014). This is due to high relaxivity, which is 10-40 times higher than commercial Gd-chelate contrast agents (CAs) (Li and Dorn, 2017) and allows sufficient image contrast at a low dose. In addition, the fullerene cage encapsulates the Gd(III) ions that would otherwise be toxic (Sosnovik and Caravan, 2013).

To achieve efficient water proton relaxation we must engineer a strong dipolar interaction between the proton's nuclear spin and the encapsulated gadolinium's unpaired electrons. Since the water molecules cannot directly coordinate to the Gd(III) ion, as in Gd-chelate CAs, the interaction must occur *via* a second-sphere or outer-sphere mechanism. This requires the

fullerene surface to be functionalised with groups containing readily exchangeable protons. Hence, polyhydroxylated and polycarboxylated derivatives of Gd@C₆₀, Gd@C₈₂ and Gd₃N@C₈₀ have been investigated most widely (Zhang *et al.*, 2014). The larger the number of functional groups attached to the surface, the higher the observed relaxivity (Zou *et al.*, 2015). Furthermore these derivatives allow the formation of aggregates by hydrogen bonding between molecules. Such aggregates, which have typical diameters of 30–150 nm, have much longer rotational correlation time than isolated molecules, giving further enhanced relaxivity (Laus *et al.*, 2007).

A number of reports have shown how the aggregation, and hence relaxivities, of Gd-EMFs can be altered either through the cage functionalisation or through changes to the aqueous environment. Dorn and co-workers made a series of polyhydroxylated Gd₃N@C₈₀ derivatives which also incorporated poly(ethylene glycol) (PEG) chains of varying lengths into the structure. Dynamic light scattering (DLS) measurements coupled with relaxivity studies revealed that the derivatives containing the shorter PEG chains (350/750 Daltons) formed larger aggregates with extremely high relaxivities, whilst those containing longer PEG chains (5000 Daltons) formed smaller aggregates with lower relaxivities at clinical-range magnetic field strengths (Zhang *et al.*, 2010).

In a similar fashion, Wang *et al.* prepared two polyhydroxylated Gd@C₈₂ derivatives containing differing numbers of hemiketal groups and demonstrated that the system with the larger number has significantly higher relaxivity (Zou *et al.*, 2015). This was ascribed to the greater capacity for this system to large aggregates by hydrogen bonding, which was confirmed by DLS measurements. Wilson and co-workers investigated the effect of pH on Gd@C₆₀(OH)_x and Gd@C₆₀[C(COOH)]₁₀ and found relaxivity to dramatically increase as pH decreased (Tóth *et al.*, 2005). This was attributed to increased aggregate stability at low pH. The same group also demonstrated that aggregates of the same derivatives were destroyed under conditions of

high salt concentration, with phosphate buffer causing the most noticeable effect (Laus *et al.*, 2005).

Sun and co-workers have recently reported a graphene oxide – Gd@C₈₂ nanohybrid in which the unfunctionalised Gd-EMF is deposited on graphene oxide nanosheets through non-covalent π - π interactions (Cui *et al.*, 2015). Interestingly, the structure was found to enhance proton relaxivity to an even greater extent than Gd@C₈₂(OH)_x despite the lack of exchangeable protons directly attached to the fullerene surface. This is apparently due to ‘secondary spin-electron transfer’ from the Gd(III) ion through the GO nanosheet onto the hydrophilic alcohol and carboxyl substituents, which in turn undergo exchange with the water protons. Maximum relaxivity was achieved by optimising the equilibrium between the conductivity of the GO nanosheet and the number of proton exchange sites present (Li *et al.*, 2016).

Presently, efforts are being made to create multimodal imaging agents, which allow multiple, complementary imaging techniques to be used on a patient simultaneously, thereby improving diagnostic capability and accuracy. The ease with which EMFs can be functionalised makes them an ideal platform to be used for the preparation of such agents. Shultz and co-workers reported a bimodal PET/MRI agent comprised of a ¹²⁴I radiolabelled carboxylated and hydroxylated Gd₃N@C₈₀ derivative (Luo *et al.*, 2012). Encouragingly the position and distribution of the agent within tumour-bearing rats was found to be comparable in both MRI and PET scans.

Gd-EMFs have also been conjugated to the exterior surface of nanoparticle systems to generate multimodal imaging agents. For example, Wang described a trimodal MRI/PET/photoacoustic imaging agent based on ⁶⁴Cu-radiolabelled polydopamine-Gd-EMF core-satellite nanoparticles (Wang *et al.*, 2017). Furthermore, the nanoparticles were loaded with doxorubicin (DOX), a widely used chemotherapy drug, which imparted them with theranostic capabilities. This was demonstrated by using a near-IR laser to induce DOX release

inside mice and completely eliminate tumors. Li et al. have developed a bimodal MR/luminescence imaging agent through the conjugation of polyhydroxylated-Gd@C₈₂-PCBM to silica-coated NaYF₄ (Y = Yb, Er) NPs (Li *et al.*, 2016). The agent displayed good relaxivity in a 7 T magnetic field, whilst a cell viability study revealed it to have minimal cytotoxicity and good biocompatibility.

In addition to the preparation of multimodal imaging systems, functionalisation of Gd-EMFs can be used to generate contrast agents with targeting capabilities. Dorn and co-workers recently reported a Gd₃N@C₈₀ derivative that targets glioblastoma multiforme (GBM) cells in mice (Li *et al.*, 2015). This was achieved through conjugation of the amino-functionalised EMF with an interleukin-13 (IL-13) peptide chain, which binds to the IL-13R α 2 receptor on the surface of GBM cells. Furthermore, the positively charged amino groups of the fullerene were found to enhance the affinity of the agent for the cell surface relative to a negatively charged carboxylate analogue, which allowed endocytosis to occur more readily.

4. Endohedral nitrogen fullerenes: towards quantum information applications.

Quantum computers that exploit the fundamental physical laws of superposition and entanglement would enormously accelerate important calculations that are intractable to existing classical computers (Mermin2012). To make such a computer, we need physical objects whose quantum states can be preserved and manipulated with high precision. Electron spins in Group V endohedral fullerenes may be one such object (Harneit2002, Benjamin2008), and N@C₆₀ has been particularly well-studied for this purpose because of its excellent quantum coherence and the possibility of incorporating into nanoscale electronic devices.

A spin-based quantum computer encodes each quantum bit (qubit) in two spin energy levels with different M_S quantum numbers. By applying microwave bursts using the technique of EPR, we can create quantum superpositions of these two states; we can think of these bursts

as rotating the spin axis relative to the static magnetic field. The first step to creating a molecular qubit is to find a pair of well-defined energy levels, which requires a detailed understanding of the electron and nuclear spin states.

In N@C₆₀, the spin states are identical to those of atomic nitrogen. Three unpaired *p* electrons combine to give electron spin quantum number $S = 3/2$. The resulting Hamiltonian is:

$$\mathcal{H} = \mu_B \mathbf{B} \mathbf{g} \mathbf{S} + \mu_N \mathbf{B} \mathbf{g}_N \mathbf{I} + \mathbf{S} \mathbf{A} \mathbf{I} + \mathbf{S} \mathbf{D} \mathbf{S}. \quad \text{Eq.2.1}$$

The first two terms describe the Zeeman coupling to the magnetic field \mathbf{B} , with the first term arising from the electron spin (with spin operator \mathbf{S} and gyromagnetic tensor \mathbf{g}) and the second term arising from the nuclear spin (with spin operator \mathbf{I} and gyromagnetic tensor \mathbf{g}_N). The third term describes hyperfine coupling between the electron and nuclear spins, parameterized by the hyperfine tensor \mathbf{A} , and the fourth term describes electron spin quadrupole coupling parameterized by the zero-field splitting (ZFS) tensor \mathbf{D} . Here μ_B is the Bohr magneton and μ_N is the nuclear magneton.

For N@C₆₀, it is an excellent approximation to assume spherically symmetric confinement, in which case the tensors in Eq. (2.1) become scalars and the zero-field splitting vanishes. Furthermore, the first term will always dominate over the second term, and in most experiments the magnetic field is set large enough that it also dominates over the third. For ¹⁴N@C₆₀, this leads to the energy levels shown in Figure 5(b). The resulting EPR spectrum (Figure 5(a)) shows three resonances, each corresponding to a different nuclear spin projection m_I . A fine scan over each resonance (Figure 5(c)) shows substructure arising partly from the hyperfine interaction in second order, and partly from coupling (not included in Eq. (2.1)) to ¹³C nuclear spins in the cage.

The scans in Figure 5(c) show how exceptionally sharp the EPR transitions can be in this material (Morton, J. J. L. 2006). This reflects the long electron spin lifetime, which is enabled by the structural symmetry of the molecule and the protection inside the cage (Knapp, C. 1997).

For quantum computing, the most important lifetime is the decoherence time T_2 (also called the transverse relaxation time (Schweiger; A. 2001)), which measures how long a quantum state can be preserved for. For carefully prepared solutions of $^{14}\text{N}@C_{60}$, this time can reach as long as $T_2 = 70 \mu\text{s}$ at room temperature, or $T_2 = 250 \mu\text{s}$ when cooled to 170 K (Morton2006). This is among the longest coherence times for any molecular radical, surpassed only by $(d_{20}\text{-Ph}_4\text{P})_2[\text{V}(\text{C}_8\text{S}_8)_3]$, Remarkably, at 10 K, the value of T_2 is 2 orders of magnitude greater than for the other solvent systems, with $T_2 = 675(7) \mu\text{s}$ ($\sim 0.7 \text{ ms}$) in CS_2 . (Zadrozny, J. M. 2015) The electron coherence time of $\text{N}@C_{60}$ appears to be ultimately limited by Orbach relaxation, i.e. the interaction of the electron spin with phonons in the cage. (Morton, J. J. L. 2006, Weil, J. 2007). Even longer coherence times can be attained when the quantum state is transferred from the electron spins to the nuclear spins (Brown, R. M. 2011).

Quantum information processing requires more than isolated qubits. If fullerene qubits are to be coupled to one another, chemical reactions are needed to rationally modify and covalently link ENFs. A set of chemical functionalization of ENFs has now been established (Zhou, S. 2015). One price of functionalising the cage is that one breaks spherical symmetry, thereby introducing significant ZFS. This introduces drawbacks, such as extra spin relaxation paths (Morton, J. J. L. 2006), but also potential advantages, such as additional EPR transitions that allow the molecule to be used as a qubit, i.e. a system encoding more than one qubit of information (Gedik, Z. 2015).

The strength of the ZFS is quantified by a traceless second-order tensor \mathbf{D} , which could be expressed as a diagonal matrix in its eigenframe with elements being $D_{xx} = -D/3 + E$, $D_{yy} = -D/3 - E$ and $D_{zz} = 2D/3$, where D and E are the ZFS parameters representing the axial and the non-axial component of the tensor. For typical cycloaddition products of ENFs, D is around 10 MHz and E is normally smaller than 1 MHz. Compared with other paramagnetic molecules, the ZFS effect is typically small. In addition to ZFS, dipolar coupling

with a strength larger than 2.67 MHz between an N@C₆₀ moiety and another covalently linked spin centre has been reported (Farrington, B. J. 2012, Zhou, S. 2016). The implementation of controllable dipolar coupling with ENFs paves the way towards interacting qubits, which is required by quantum information applications.

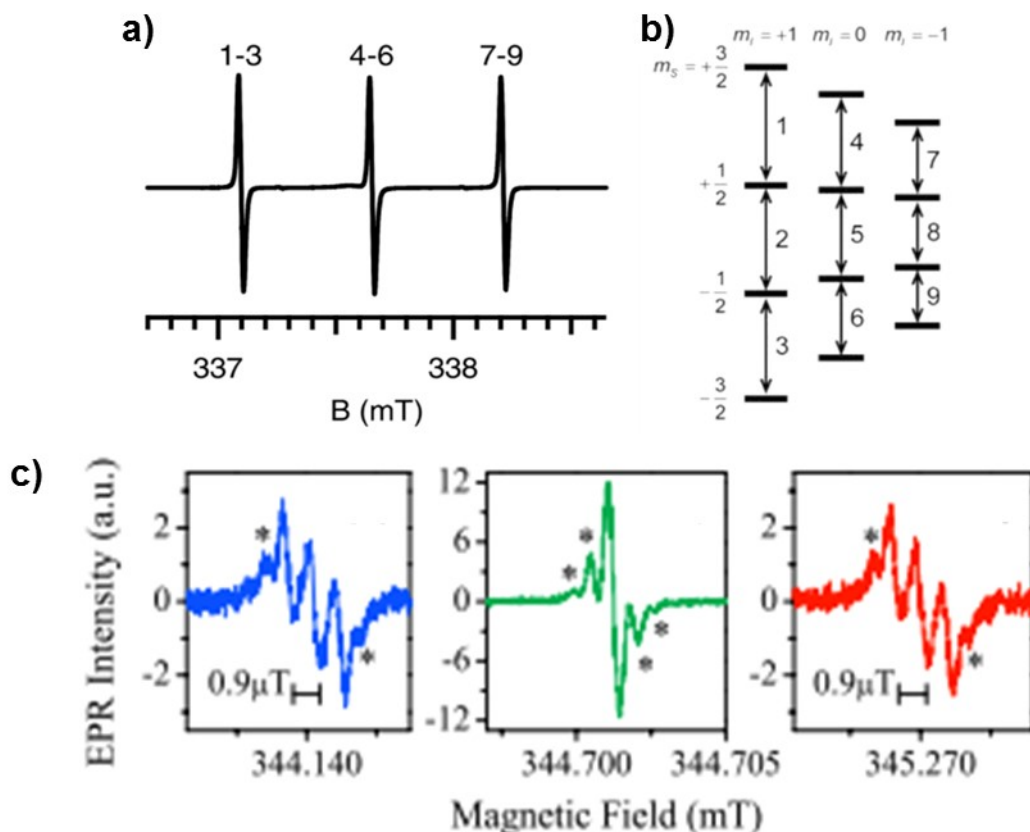


Figure 5. (a) EPR spectrum of N@C₆₀ diluted in C₆₀ powder. (b) Energy levels and allowed transitions of ¹⁴N@C₆₀ in the high field limit. For each of three possible nuclear spin alignments m_I , there is a ladder of four electron spin levels. Hyperfine coupling gives each ladder a different energy spacing. (c) Zoom-in for each of the three resonances (blue: $m_I = +1$, green: $m_I = 0$, red: $m_I = -1$), showing the sharp linewidth and the second order hyperfine pattern. (Asterisks denote resonances arising from coupling to cage ¹³C spins.) Panels a and b from (Harneit, W. 2006). Panel c from (Morton, 2006).

5. Atomic clocks: fullerenes as frequency standards.

Many modern technologies, such as communications and navigation, rely on precise and stable frequency standards (Vig 1993). For example, high frequency stability is necessary in communication systems to ensure that the transmitter and receiver remain synchronised. This is particularly important for jamming-resistant communications that work by coordinated hopping over different frequencies. In navigation applications, such as global navigation satellite system (GNSS) receivers, high-stability frequency standards could improve positional accuracy in signal-degraded environments (Misra 1996). The most stable clocks work by locking an electronic oscillator to a reference frequency provided by an atomic transition (Riehle 2004) as shown in Figure 6 (a). Since atomic transition frequencies are fixed by nature, this reduces the influence of manufacturing variation and drift and results in a highly stable and reproducible output frequency. Such a system is commonly called an “atomic clock”. For portable atomic clocks, size, weight and power (SWaP) are important parameters in addition to stability (Vig 1993).

The state-of-the-art miniaturised atomic frequency standard is the chip scale atomic clock (CSAC) (Knappe 2004). Such a clock operates by disciplining a local oscillator to the magnetic resonance signal of an optically-probed alkali metal vapour, which is confined in a vacuum chamber. Microelectromechanical (MEM) fabrication allows construction of miniature vacuum chambers with integrated diode lasers and optical sensors, leading to commercially available atomic clocks with a total volume less than 17cm^3 (Microsemi Corporation 2017). However, CSACs suffer long-term drifts caused by changing buffer gas pressure as the vapour cell ages. Moreover, further reduction of SWaP is necessary for broader adoption of portable atomic clocks (Lutwak 2007). Another drawback is that some applications require robustness against acceleration and vibration (Vig 1993), which is limited by the vacuum packaging that thermally isolates the vapour cell (Lutwak 2007).

These problems may be solvable using frequency references based on condensed-matter systems, which obviate the need for the vapour cell. Proposed examples include V^{++} in MgO (White 2005), and nitrogen vacancies in diamond (Hodges 2014). However, in neither system has the necessary stability been demonstrated experimentally. For both these proposed frequency standards, the minimum resonance linewidth, and hence maximum stability, is limited by inhomogeneous broadening due to lattice strains.

Here we describe an alternative condensed-matter clock material: the Group V-containing endohedral fullerenes (Briggs 2012). In contrast to vapour-based clocks, which use optical interrogation of the spin ensemble, the proposed fullerene-based clocks use radio-frequency (rf) measurement of the endohedral fullerene's EPR spectrum. As mentioned previously, resonances as narrow as $0.3 \mu\text{T}$ have been observed at the X band in a carefully prepared sample (Morton 2006). The importance of narrow resonances for a clock can be intuitively understood by considering them analogous to the markings on a ruler: the sharper the resonances, the more precisely the frequency can be measured.

Sharp resonances are a necessary but not sufficient condition for the frequency reference in an atomic clock. It is also necessary to select a transition whose frequency is insensitive to environmental noise (Audoin 1976). For example, all atomic clocks use “clock transitions”, which are resonances with the property that their frequency f is first-order independent of magnetic field B : i.e. $df/dB = 0$. If B is set to the clock field B_{clock} at which such a clock transition exists, then small external magnetic fields barely perturb the clock frequency. At this clock field, the transition frequency is fixed by the isotropic hyperfine coupling constant A .

Such a clock transition has long been predicted for $^{15}\text{N}@C_{60}$ (Briggs 2012). As seen from Figure 6 (b), at a magnetic field of approximately 8 G, two of the spin energy levels run parallel, implying that the frequency of the transition between them satisfies the clock condition $df/dB = 0$. Experimental verification has been challenging due to its low frequency, which

leads to a small spin polarisation and weak signal. Recently, the clock transition has been measured using a custom built low-field EPR spectrometer (Harding 2017), as shown in Figure 6 (d). Given advances in spectrometer miniaturisation developed for “1-chip” NMR (Sun 2011) a fullerene-based clock on an integrated circuit seems feasible.

One can predict the stability of an atomic clock by considering the frequency of the clock transition, the observed resonance linewidth, and the signal-to-noise ratio (SNR) of the resonance (Riehle 2004). Current measurements on fullerene-based systems imply a stability that is approximately seven orders of magnitude worse than existing chip-scale atomic clocks (Knappe 2004). However, there is scope for improvement by spectrometer and sample optimisation, which could improve SNR and linewidth. The most significant improvements would likely come from sample purification to increase the spin density, and hence signal strength, or from reduction of the resonance linewidth. It is reasonable to expect an improvement to the linewidth, since the current value is approximately one order of magnitude worse than has been achieved in the literature. Furthermore, improved coherence times at the clock field have been observed in other systems, due to improved immunity to dipolar decoherence (Shiddiq 2016), which indicates a potential for reduced linewidth at the clock field. Therefore, a fullerene-based clock could potentially be competitive with CSACs while achieving reduced SWaP. Furthermore, use of $^{31}\text{P}@C_{60}$ may permit further improvements due to its larger hyperfine coupling, which increases the clock transition frequency.

For long-term clock stability, it is also necessary to suppress frequency drifts caused by temperature fluctuations. These arise because the hyperfine constant of $\text{N}@C_{60}$ depends on temperature, with a relative shift of $(1/A)[dA/dT] \approx 100$ ppm/K (Pietzak 2002). It will be necessary either to stabilise the temperature of the sample cell or to compensate for this effect. One possibility is to offset the temperature dependence with a second control parameter such

as pressure (Hodges 2014). Another possibility is again to use $^{31}\text{P}@C_{60}$, which has a weaker temperature dependence (Pietzak 2002).

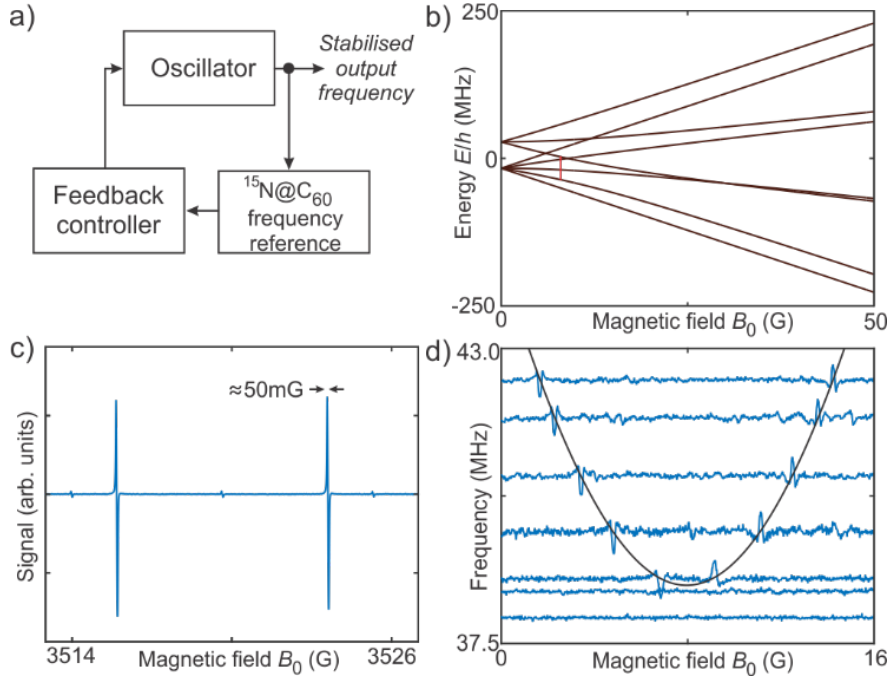


Figure 6. (a) Schematic of atomic clock using $^{15}\text{N}@C_{60}$ as the frequency reference. A radio signal generated by a local oscillator is used to probe a $^{15}\text{N}@C_{60}$ sample. The response of the sample is used for feedback to lock the frequency of the oscillator to the EPR resonance. (b) Low field energy levels as a function of magnetic field. The clock transition (vertical red line) occurs in the region where the Zeeman energy is comparable to the hyperfine coupling. (c) X-band spectrum of $^{15}\text{N}@C_{60}$, showing clearly narrow resonance signals. (d) Field-frequency map of the clock transition frequency as a function of magnetic field, demonstrating $df/dB = 0$ at the clock field $B_{\text{clock}} \approx 0.8$ mT. Based on the work by Harding 2017.

6. Perspectives

While the well-known drawbacks of endohedral metallofullerenes and nitrogen containing endohedral fullerenes such as their low production yield and tedious purification processes remain unanswered, recent developments in the field, including the chemically activated reaction atmosphere, chemical doping of the graphite rods and the Lewis acid selective precipitation methods, provide hope for the scaled-up production of this class of exotic materials. The synthesis and surface functionalization of novel dimetallic EMFs that will exhibit stronger magnetization can present an important milestone regarding the applications of these materials as also the development of phosphorus containing endohedral fullerenes for atomic clocks applications.

The conclusion is that the future of research in endohedral fullerenes and their derivatives is looking bright!

References.

- Zhao, J. et al. 2015 *Coord.Chem.Rev.* 289-290: 315
- Roukala, J. et al. 2017 Ratcheting rotation or speedy spinning: EPR and dynamics of $\text{Sc}_3\text{C}_2@\text{C}_{80}$ *Chem.Commun.* 53: 8992
- Wu, B et al. 2015 Molecular magnetic switch for a metallofullerene *Nat.Commun.* 6468
- Inakuma, M. Shinohara, H. 2000 Structural and Electronic Properties of Isomers of $\text{Sc}_2@\text{C}_{84}$ (I, II, III): ^{13}C NMR and IR/Raman Spectroscopic Studies *J.Phys.Chem.B.* 104: 7595
- Elliott, B. et al. 2013 Spin Density and Cluster Dynamics in $\text{Sc}_3\text{N}@\text{C}_{80}$ – upon [5,6] Exohedral Functionalization: An ESR and DFT Study *J.Phys.Chem.C.* 117: 2344

- Hajjaj, F. et al. 2011 Ferromagnetic Spin Coupling between Endohedral Metallofullerene La@C₈₂ and a Cyclodimeric Copper Porphyrin upon Inclusion *J.Am.Chem.Soc.* 133: 9290
- Svitova, A.L., Krupskaya, Y., Samoylova, N., Kraus, Geck, R., Dunsch, L., Popov, A.A. 2014 Magnetic moments and exchange coupling in nitride clusterfullerenes Gd_xSc_{3-x}N@C₈₀ (x = 1–3) *Dalton Trans.*; 43: 7387
- Hermanns, C.F. et al. 2013 Magnetic coupling of Gd₃N@C₈₀ endohedral fullerenes to a substrate *Phys.Rev.Lett.*; 111: 167203
- Brown, R.M. et al. 2010 *Phys.Rev.B.* Electron spin coherence in metallofullerenes: Y, Sc, and La@C₂₈; 82: 033410
- Cui, Rongli, Li, J., Huang, H., Zhang, M., Guo, X., Chang, Y., et al. (2015). Novel Carbon Nanohybrids as Highly Efficient Magnetic Resonance Imaging Contrast Agents. *Nano Research.* 8: 1259–1268
- Ghiassi, K. B., Olmstead, M. M., and Balch, A. L. 2014 Gadolinium-Containing Endohedral Fullerenes: Structures and Function as Magnetic Resonance Imaging (MRI) Agents. *Dalton Transactions.* 43: 7346–7358
- Laus, S., Sitharaman, B., Tóth, É., Bolskar, R. D., Helm, L., Asokan, S., et al. (2005). Destroying Gadofullerene Aggregates by Salt Addition in Aqueous Solution of Gd@C₆₀(OH)_x and Gd@C₆₀[C(COOH₂)]₁₀. *Journal of the American Chemical Society.* 127: 9368–9369
- Laus, S., Sitharaman, B., Tóth, É., Bolskar, R. D., Helm, L., Wilson, L. J., et al. 2007 Understanding Paramagnetic Relaxation Phenomena for Water-Soluble Gadofullerenes. *The Journal of Physical Chemistry C.* 111: 5633–5639

- Li, C., Cui, R., Feng, L., Li, J., Huang, H., Yao, H., *et al.* 2016 Synthesis of a UCNPs@SiO₂@gadofullerene Nanocomposite and Its Application in UCL/MR Bimodal Imaging. *RSC Advances*. 6: 98968–98974
- Li, J., Cui, R., Chang, Y., Guo, X., Gu, W., Huang, H., *et al.* 2016 Adaption of the Structure of Carbon Nanohybrids toward High-Relaxivity for a New MRI Contrast Agent. *RSC Advances*. 6: 58028–58033
- Li, T., and Dorn, H. C. 2017 Biomedical Applications of Metal-Encapsulated Fullerene Nanoparticles. *Small*. 13: 1603152
- Li, T., Murphy, S., Kiselev, B., Bakshi, K. S., Zhang, J., Eltahir, A., *et al.* 2015 A New Interleukin-13 Amino-Coated Gadolinium Metallofullerene Nanoparticle for Targeted MRI Detection of Glioblastoma Tumor Cells. *Journal of the American Chemical Society*. 137: 7881–7888
- Luo, J, Wilson, J. D., Zhang, J., Hirsch, J. I., Dorn, H. C., Fatouros, P. P., *et al.* 2012 A Dual PET/MR Imaging Nanoprobe: 124I Labeled Gd₃N@C₈₀. *Applied Sciences*. 2: 465–478
- Mikawa, M., Kato, H., Okumura, M., Narazaki, M., Kanazawa, Y., Miwa, N., *et al.* (2001). Paramagnetic Water-Soluble Metallofullerenes Having the Highest Relaxivity for MRI Contrast Agents. *Bioconjugate Chemistry*. 12: 510–51
- Sosnovik, D. E., and Caravan, P. 2013 Molecular MRI of the Cardiovascular System in the Post-NSF Era. *Current Cardiovascular Imaging Reports*. 6: 61–68
- Tóth, É, Bolskar, R. D., Borel, A., González, G., Helm, L., Merbach, A. E., *et al.* (2005). Water-Soluble Gadofullerenes: Toward High-Relaxivity, PH-Responsive MRI Contrast Agents. *Journal of the American Chemical Society*. 127: 799–805

- Wang, S., Lin, J., Wang, Z., Zhou, Z., Bai, R., Lu, N., *et al.* (2017). Core–Satellite Polydopamine–Gadolinium-Metallofullerene Nanotheranostics for Multimodal Imaging Guided Combination Cancer Therapy. *Advanced Materials*. 29: 1701013
- Zhang, J., Fatouros, P. P., Shu, C., Reid, J., Owens, L. S., Cai, T., *et al.* (2010). High Relaxivity Trimetallic Nitride (Gd₃N) Metallofullerene MRI Contrast Agents with Optimized Functionality. *Bioconjugate Chemistry* 21: 610–615
- Zhang, J., Ye, Y., Chen, Y., Pregot, C., Li, T., Balasubramaniam, S., *et al.* (2014). Gd₃N@C₈₄(OH)_x: A New Egg-Shaped Metallofullerene Magnetic Resonance Imaging Contrast Agent. *Journal of the American Chemical Society*. 136: 2630–2636
- Zou, T, Zhen, M., Li, J., Chen, D., Feng, Y., Li, R., *et al.* (2015). The Effect of Hemiketals on the Relaxivity of Endohedral Gadofullerenols. *RSC Advances*. 5: 96253–96257.
- Vig, J.R., 1993 "Military applications of high accuracy frequency standards and clocks," *IEEE Trans. Ultrason. Ferroelectr. Freq. Control*, 40: 522,
- Misra, P., 1996 "The Role of the Clock in a GPS receiver," *GPS World*, 60-66
- Riehle, F. Frequency Standards: Basics and Applications, Weinheim, Germany: Wiley, 2004.
- Microsemi Corporation, 2017 "Quantum™ SA.45s CSAC chip scale atomic clock," Aliso Viejo, California, USA.
- Lutwak, R., Rashed, A., Varghese, M., et al, 2007 "The chip-scale atomic clock--prototype evaluation," in Proceedings of the 36th Annual Precise Time and Time Interval Systems and Applications Meeting, Kona, Hawaii, USA.
- White. C.J., Hajimir, A. 2005 "A solid-state atomic frequency standard," in *Proc. IEEE Internat. Freq. Control Symp. Exp.*, Vancouver, Canada.

- Hodges, J.S., Yao, N.Y., Maclaurin, D., Rastogi, C., Lukin, M.D., Englund, D. 2014 "Timekeeping with electron spin states in diamond," *Phys. Rev. A.* 87: 032118.
- Briggs, G.A.D., Ardavan, A, 2012 "US Patent No 8,217,724,"
- Almeida Murphy, T., Pawlik, T., Weidinger, A., et al, 1996 "Observation of Atom like Nitrogen in Nitrogen-Implanted Solid C₆₀," *Phys. Rev. Lett.* 77: 1075-1078
- Knapp, C., Dinse, K.P., Pietzak, B., Waiblinger, M., Weidinger, A. 1997 "Fourier transform EPR study of N@C₆₀ in solution," *Chem.Phys.Lett*, 272: 433-437
- Morton, J.J.L., Tyryshkin, A.M., Ardavan, A., Porfyrakis, K., Lyon, S.A., Briggs, G.A.D, 2006 "Electron spin relaxation of N@C₆₀ in CS₂," *J.Chem.Phys.* 124: 014508.
- Audoin, C., Vanier, J. 1976 "Atomic frequency standards and clocks," *Journal of Physics E: Scientific Instruments* 9: 697-720.
- Harding, R.T., Zhou, S., Zhou, J. et al. 2017 "Spin Resonance Clock Transition of the Endohedral Fullerene ¹⁵N@C₆₀," *Phys. Rev. Lett.*
- Sun, N., Yoon, T.J., Lee, H., Andress, W., Weissleder, R., Ham, D. 2011 "Palm NMR and 1-chip NMR," *IEEE Journal of Solid-State Circuits*, 46: 342-352.
- Shiddiq, M., Komijani, D., Duan, Y., Gaita-Arino, A., Coronado, E., Hill, S. 2016 "Enhancing coherence in molecular spin qubits via atomic clock transitions," *Nature*, 531: 348-351.
- Knapp, C., Weiden, N., Kass, H., Dinse, K.P., Pietzak, B., Waiblinger, M., Weidinger, A. 1998 "Electron paramagnetic resonance study of atomic phosphorus encapsulated in [60] fullerene," *Mol. Phys.* 95: 999-1004.
- Pietzak, B., Weidinger, A., Dinse, K.P., Hirsch, A. 2002 "Group V Endohedral Fullerenes: N@C₆₀, N@C₇₀, and P@C₆₀," in *Endofullerenes: A New Family of Carbon Clusters*, Springer.
- Benjamin, S. C. *et al.* 2006 Towards a fullerene-based quantum computer. *J. Phys.*

Condens. Matter **18**: S867–S883.

- Bartl, A. & Dunsch, L. 2001 Temperature dependent metal cluster position inside a C₈₂ cage: Sc₃@C₈₂. *Synth. Met.* **121**: 1147–1148.
- Cirić, L. *et al.* 2008 La@C₈₂ as a spin-active filling of SWCNTs: ESR study of magnetic and photophysical properties. *Phys. Status Solidi Basic Res.* **245**: 2042–2046.
- Kitaura, R., Okimoto, H., Shinohara, H., Nakamura, T. & Osawa, H. 2007 Magnetism of the endohedral metallofullerenes M@C₈₂ (M=Gd,Dy) and the corresponding nanoscale peapods: Synchrotron soft x-ray magnetic circular dichroism and density-functional theory calculations. *Phys. Rev. B - Condens. Matter Mater. Phys.* **76**, 1–4.
- Koltover, V. K. 2004 Spin-leakage of the fullerene shell of endometallofullerenes: EPR, ENDOR and NMR evidences. *Carbon N. Y.* **42**: 1179–1183.
- Koltover, V. K. *et al.* 2004 Diamagnetic clusters of paramagnetic endometallofullerenes: A solid-state MAS NMR study. *J. Phys. Chem. B* **108**: 12450–12455.
- Theobald, J. A., Oxtoby, N. S., Phillips, M. A., Champness, N. R. & Beton, P. H. 2003 Controlling molecular deposition and layer structure with supramolecular surface assemblies. *Nature* **424**: 1029–1031
- Chen C-H, Krylov D.S, Avdoshenko S.M, Liu F, Spree L, Yadav R, Alvertis A, Hozoi L, Nenkov K, Kostanyan A, Greber T, Wolter AUB, Popov AA. 2017 Selective arc-discharge synthesis of Dy₂S-clusterfullerenes and their isomer-dependent single molecule magnetism. *Chem.Sci.*, **8**: 6451-6465
- Harneit, W., Huebener, K., Naydenov, B., Schaefer, S. & Scheloske, M. 2007 N@C₆₀ quantum bit engineering. *Phys. Status Solidi* **244**: 3879–3884.
- B.Wu, Y.Li, L.Jiang, C.Wang, T.Wang, 2016 “Spin-Paramagnet between Nitroxide Radical and Metallofullerene” *J. Phys. Chem. C.* **120**(11): 6252–6255

- Bondino, F. Cepek, C. Tagmatarchis, N. Prato, M. Shinohara, H. Goldoni, A. 2006 Element-Specific Probe of the Magnetic and Electronic Properties of Dy incarcerated Fullerenes. *J. Phys. Chem. B.* 110: 7289–7295.
- Li, Y., Wang, T., Zhao, C., Qin, Y., Meng, H., Nie, M., Jiang, L., Wang, C. 2017 A magnetoreception system constructed by a dysprosium metallofullerene and nitroxide radical. *Dalton Trans. Dalton Trans.* 46: 8938
- Murphy, T. A. Pawlik, T. Weidinger, A. et al. 1996 Observation of Atomlike Nitrogen in Nitrogen-Implanted Solid C₆₀, *Phys. Rev. Lett.* 77: 1075.
- Pietzak, B. Waiblinger, M. Murphy, T. A. et al. 1997 Buckminsterfullerene C₆₀: a chemical Faraday cage for atomic nitrogen, *Chem. Phys. Lett.* 4: 259.
- Cho, S. C. Kaneko, T. Ishida, H. et al. 2015 Nitrogen-atom endohedral fullerene synthesis with high efficiency by controlling plasma-ion irradiation energy and C₆₀ internal energy. *J. Appl. Phys.* 117: 123301.
- Zhou S, Rasovic I, Briggs GAD, Porfyrakis K. 2015 Synthesis of the first completely spin-compatible N@C₆₀ cyclopropane derivatives by carefully tuning the DBU base catalyst, *Chem. Commun.* 51: 7096-7097
- Farrington, B. J., Jevric, M., Rance, G. A., Ardavan, A., Khlobystov, A. N., Briggs, G. A. D., Porfyrakis, K. 2012 Chemistry at the Nanoscale: Synthesis of an N@C₆₀-N@C₆₀ Endohedral Fullerene Dimer *Angew. Chem. Int. Ed.* 51 (15): 3587
- Zhou S, Yamamoto M, Briggs GAD, Imahori H, Porfyrakis K. 2016 Probing the Dipolar Coupling in a Heterospin Endohedral Fullerene– Phthalocyanine Dyad, *J. Am. Chem. Soc.* 138: 1313-1319
- Gedik, Z., Silva, I. A., 2015 Çakmak, B., Karpat, G., Vidoto, E. L. G., Soares-Pinto, D. O., DeAzevedo, E. R., Fanchini, F. F. *Sci. Rep.* 5: 1.

- Morton, J. J. L., Tyryshkin, A. M., Ardavan, A., Porfyraakis, K., Lyon, S. A., Briggs, G. A. D. 2006 Electron spin relaxation of N@C₆₀ in *J.Chem.Phys.* 124 (1): 14508.
- Laird, E.A, Pei, F, Kouwenhoven L.P. 2013 *Nat. Nanotechnol.* 8: 565
- Mermin 2007 "Quantum Computer Science", Cambridge University Press
- Pietzak B, Waiblinger M, Almeida Murphy T, Weidinger A, Hohne M, Dietel E, Hirsch A, 1998 "Properties of Endohedral N@C₆₀ *Carbon* 36: 613-615
- Knapp C, Weiden N, Kass H, Dinse K-P, Waiblinger M, Weidinger A. 1998 "Electron paramagnetic resonance study of atomic phosphorus encapsulated in [60]fullerene," *Molecular Physics* 95: 999-1004
- Inakuma M, Shinohara H. 2000 "Temperature-Dependent EPR Studies on Isolated Scandium Metallofullerenes: Sc@C₈₂(I, II) and Sc@C₈₄," *J. Phys. Chem. B* 104: 7595-7599
- Kikuchi K, Nakao Y, Suzuki S, Achiba Y, Suzuki T, Maruyama Y. 1994 "Characterization of the Isolated Y@C₈₂," *J. Am. Chem. Soc.* 116: 9367-9368.
- Yamamoto K, Funasaka H, Takahashi T, Akasaka T, 1994 "Isolation of an ESR-Active Metallofullerene of La@C₈₂," *J. Phys. Chem.*, 98(8): 2008-2011.
- Shinohara H, Inakuma M, Hayashi N, Sato H, Saito Y, Kato T, Bandow S. 1994 "Spectroscopic Properties of Isolated Sc₃@C₈₂ Metallofullerene," *J. Phys. Chem.* 98(35): 8597.
- Zadrozny J. M., Niklas J, Poluektov O.G., 2015 Freedman D.E. *ACS Cent.Sci.* 1: 488